JACS
JOURNAL OF THE AMERICAN CHEMICAL SOCIETY
Article
pubs.acs.org/JACS

Molecularly Tunable Fluorescent Quantum Defects

Hyejin Kwon,[†] Al'ona Furmanchuk,[‡,§] Mijin Kim,[†] Brendan Meany,[†] Yong Guo,[∥] George C. Schatz,[*,‡] and YuHuang Wang[*,†,⊥]

[†]Department of Chemistry and Biochemistry, University of Maryland, College Park, Maryland 20742, United States
[‡]Department of Chemistry, Northwestern University, 2145 Sheridan Road, Evanston, Illinois 60208, United States
[§]Department of Electrical Engineering and Computer Science, Northwestern University, 2145 Sheridan Road, Evanston, Illinois 60208, United States
[∥]Key Laboratory of Organofluorine Chemistry, Shanghai Institute of Organic Chemistry, Chinese Academy of Sciences, Shanghai 200032, China
[⊥]Maryland NanoCenter, University of Maryland, College Park, Maryland 20742, United States

Supporting Information

ABSTRACT: We describe the chemical creation of molecularly tunable fluorescent quantum defects in semiconducting carbon nanotubes through covalently bonded surface functional groups that are themselves nonemitting. By variation of the surface functional groups, the same carbon nanotube crystal is chemically converted to create more than 30 distinct fluorescent nanostructures with unique near-infrared photoluminescence that is molecularly specific, systematically tunable, and significantly brighter than that of the parent semiconductor. This novel exciton-tailoring chemistry readily occurs in aqueous solution and creates functional defects on the sp^2 carbon lattice with highly predictable C−C bonding from virtually any iodine-containing hydrocarbon precursor. Our new ability to control nanostructure excitons through a single surface functional group opens up exciting possibilities for postsynthesis chemical engineering of carbon nanomaterials and suggests that the rational design and creation of a large variety of molecularly tunable quantum emitters—for applications ranging from in vivo bioimaging and chemical sensing to room-temperature single-photon sources—can now be anticipated.

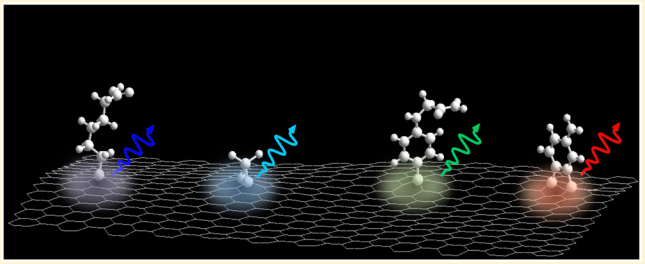

INTRODUCTION

The excited states of many semiconducting nanocrystals and polymers are characterized by excitons, electron−hole pairs bound by Coulomb interactions.[1] Excitons are hydrogen-atom-like quasi-particles, each carrying a quantum of electronic excitation energy. An exciton can return to the ground state by emitting a photon, producing photoluminescence (PL), or by falling into a "dark" state from which the energy is lost as heat. The ability to control the fate of excitons and their energy is crucial to imaging,[2,3] sensing,[4] photovoltaics,[5] lighting and displays,[6] and many other important electronic functions.

Over the last few decades, two major classes of approaches, quantum confinement and doping, have been developed to tailor the exciton properties within a nanocrystal. When a nanocrystal becomes smaller than the Bohr radius of excitons, the electronic wave function becomes confined, leading to the existence of discrete energy levels that are strongly dependent on the size of the nanocrystal.[7,8] This quantum confinement effect has motivated the development of many innovative synthetic approaches that control the size and shape of nanocrystals and consequently their electronic and optical properties.[9] The other approach is doping of inorganic semiconductor nanocrystals by the incorporation of atomic impurities as color centers into the crystal lattice. Examples include nitrogen vacancies in diamond[10] and metal-ion-doped nanocrystals.[11] In the case of single-walled carbon nanotubes (SWCNTs), the excitonic properties depend on both the diameter and chiral angle of each nanotube crystal, collectively known as the chirality, which can be denoted by a pair of integers (n,m).[12,13] The optical properties can also be modified by doping with oxygen[14] or incorporation of sp^3 defects through diazonium chemistry.[15] Excitingly, these defects can induce unique near-infrared emission,[14] brighten dark excitons,[15,16] facilitate upconversion,[17] and stabilize trions at room temperature,[18] making them particularly interesting for emergent photonic applications. However, both reported methods for defect creation are inherently bound by the limited chemical and optical tunability. In particular, oxygen doping leads to mixed ether and epoxide structures,[14,19] while diazonium chemistry only works for specific aryl groups and monovalent bonding,[15] and the reaction rates for both are low.[14,15] For these reasons, examples of this type of defect are rare, and although it has long been suggested,[15] the prospect of

Received: April 13, 2016
Published: May 9, 2016

DOI: 10.1021/jacs.6b03618
J. Am. Chem. Soc. 2016, 138, 6878−6885

using defects for materials engineering has not been demonstrated.

Here we describe a versatile new chemistry that enables direct tailoring of excitons within a single material through molecular engineering of covalently attached surface functional groups (Figure 1). We illustrate this new approach to materials

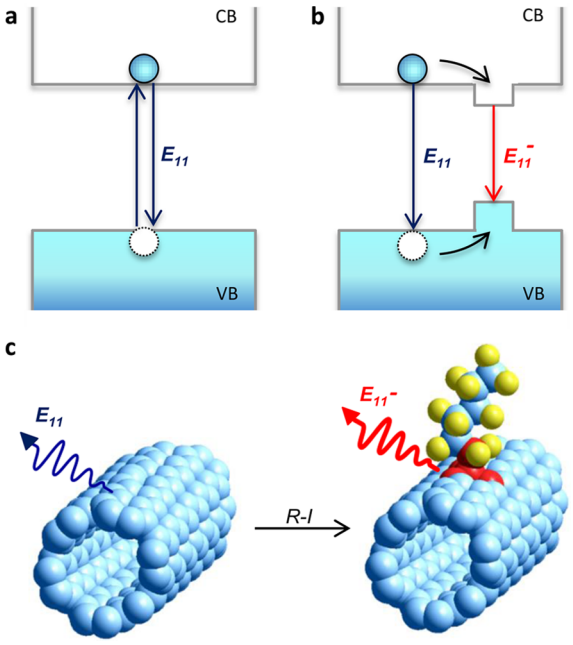

Figure 1. Fluorescent quantum defect approach to nanomaterial engineering. (a) In a quantum confinement system, the exciton wave function is confined as the particle size reaches the Bohr radius of the quasi-particle, lending the capability to control the optical properties by size engineering. (b) In the proposed quantum defect systems, the mobile excitons can be trapped and their optical properties can be controlled by molecular engineering of the trap. (c) Creation of a fluorescent quantum defect by the reaction of a SWCNT semiconductor with an iodide-containing precursor.

engineering through the synthesis of more than 30 new fluorescent nanostructures from SWCNTs of the same crystal structure by creating molecularly tunable fluorescent quantum defects in the sp^2 carbon lattice. Each of the new synthetic nanostructures may be viewed as a diamond-in-graphene structure reminiscent of an island in an electron sea. More specifically, in the case of semiconducting nanotubes, these structures can be viewed as hybrid quantum systems that allow excitation energy (carried by the exciton) to be channeled along a one-dimensional (1D) antenna and then harvested using a zero-dimensional (0D) funnel. Compared with quantum confinement, which controls the optical and electronic gap by size engineering, these fluorescent defects create local potential wells on the sp^2 lattice of SWCNTs that can be chemically tailored with molecular control as shown herein. To recognize their molecular nature and the fact that the local potential well is a result of defect-induced splitting of frontier orbitals, we propose to call these "fluorescent quantum defects". Furthermore, unlike atomic color-center dopants, our defect-inducing surface functional groups are themselves nonemitting and readily accessible chemically, thereby affording unprecedented molecular control and engineering flexibility.

These molecularly tunable fluorescent quantum defects are enabled by a versatile new chemistry that allows covalent attachment of iodine-containing hydrocarbon precursors to the sp^2 carbon lattice through highly predictable C−C bonding. The reaction occurs in aqueous solution upon mixing of an alkyl halide with nanotubes in the presence of sodium dithionite, which acts as a mild reductant.[20] We note that sidewall alkylation can occur under extreme conditions, such as in the Billups−Birch reaction, in which solvated electrons in liquid ammonia are required.[21,22] However, the new chemistry described here is significantly more versatile because molecularly tunable fluorescent quantum defects can be created with highly predictable C−C bonding points from virtually any iodine-containing hydrocarbon precursor. Notably, this exciton-tailoring chemistry is not limited to the creation of monovalent alkyl defects. Both monovalent and divalent defects can be created by reacting SWCNTs with respective alkyl or aryl iodide or diiodide precursors, respectively. In contrast to alkyl iodides, which require activation by sodium dithionite, aryl iodides alone can react with SWCNTs by resonant excitation of the nanotubes with visible light. Furthermore, the aqueous medium allows for *in situ* probing of the evolution of sidewall alkylation and provides a level of control that was previously unattainable.[14,15]

MATERIALS AND METHODS

Aqueous Dispersions of Individual SWCNT Crystals. SWCNTs (HiPco, batch no. 194.3, Rice University, or CoMoCAT SG65i, lot no. 000-0036, SouthWest NanoTechnologies, Inc.) were stabilized by 1 wt % sodium dodecyl sulfate (SDS, Sigma-Aldrich, ≥98.5%) in D_2O (Cambridge Isotope Laboratories, Inc., 99.8%) by tip ultrasonication (Misonix) at 35 W, 10 °C in a stainless steel beaker for 2 h, followed by ultracentrifugation with an Optima LE-80K ultracentrifuge (Beckman Coulter) at 170499*g* for 2 h to remove bundled nanotubes and residual catalysts. The individually dispersed SWCNTs were sorted for high purity (6,5)-SWCNTs using gel chromatography.[23] The samples were diluted to an optical density of 0.1 at the E_{11} absorption peak of (6,5)-SWCNTs in 1 wt % SDS in D_2O. The concentrations of HiPco and CoMoCAT were determined with a calibration curve from correlated optical density and thermogravimetric analysis. The concentrations of chirality-enriched solutions were calculated on the basis of the extinction coefficient previously determined by Zheng and Diner.[30]

Synthetic Creation of Fluorescent Quantum Defects in SWCNTs. Sodium bicarbonate (EMP Chemicals, ACS grade), acetonitrile (Sigma-Aldrich, 99.9%), and alkyl halides were added sequentially to each SWCNT solution, which was kept in a capped glass vial covered with aluminum foil. Acetonitrile was used as a cosolvent for the alkyl halide. Sodium dithionite (Sigma-Aldrich, 85%) was then added to the mixture, which was stirred with a magnetic stir bar at room temperature. For aryl defects, only aryl-containing iodides are required, and the reaction was triggered by optical excitation of the E_{22} transition of the nanotubes. The degree of functionalization was controlled by adjusting the relative amounts of the reagents. The reactions were monitored at various times by UV−vis−NIR absorption and fluorescence spectroscopy.

In Situ UV−Vis−NIR Absorption and Photoluminescence Spectroscopy. The reactions were monitored in situ using a Lambda 1050 UV−vis−NIR spectrophotometer (PerkinElmer) equipped with both a photomultiplier tube detector and an extended InGaAs detector and a NanoLog spectrofluorometer (Horiba Jobin Yvon). For fluorescence spectroscopy, the samples were excited with a 450 W xenon source dispersed by a double-grating monochromator. Excitation−emission maps and fluorescence spectra were collected using a liquid-N_2-cooled linear InGaAs array detector on a 320 mm imaging spectrometer. The spectrofluorometer was calibrated against NIR emission lines of a pencil-style neon spectral calibration lamp (Newport). Absorption and PL spectra were fitted with Voigt functions using PeakFit software version 4.12. No baseline correction

DOI: 10.1021/jacs.6b03618
J. Am. Chem. Soc. 2016, 138, 6878−6885

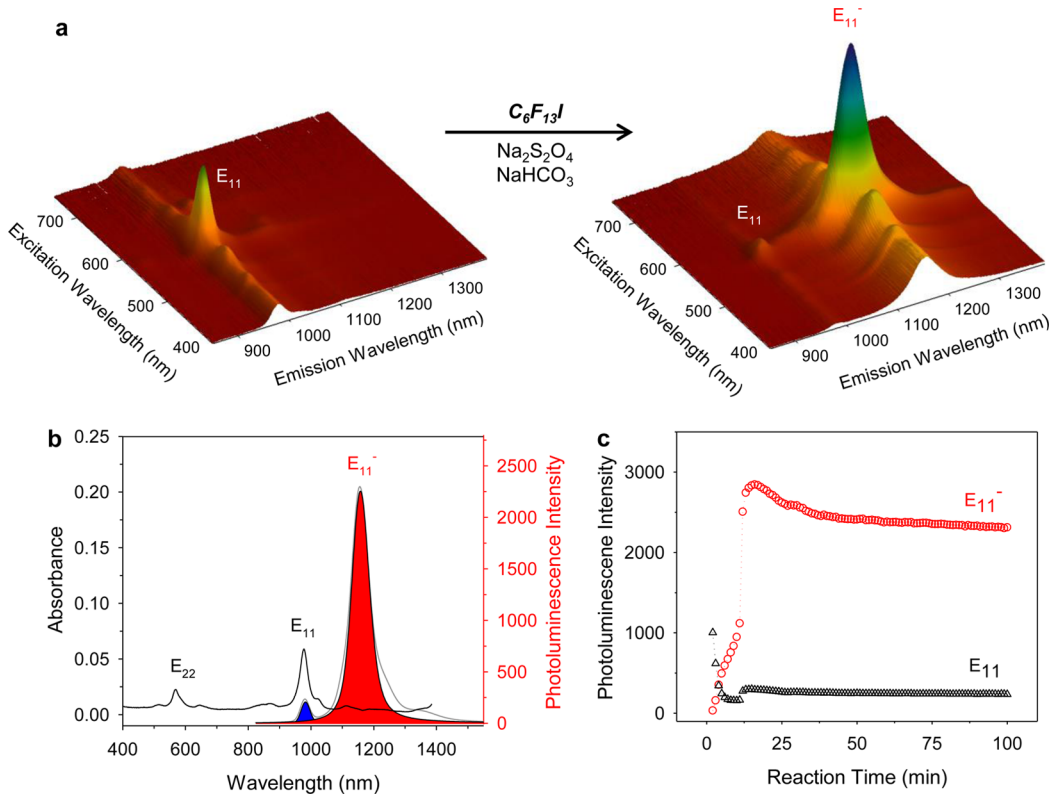

Figure 2. Chemical creation of fluorescent (6,5)-SWCNT−$CF_2(CF_2)_5CF_3$. (a) Defect photoluminescence arises farther in the near-infrared (NIR), 190 meV to the red of the parent nanotube excitonic emission. (b) Correlated vis−NIR absorption (black line) and PL (red line) spectra for (6,5)-SWCNT−$CF_2(CF_2)_5CF_3$. The SWCNTs were excited at the E_{22} transition (565 nm). (c) Evolution of the E_{11} and E_{11}^- emissions. The intensity of the E_{11}^- emission reached the maximum after 12 min of reaction and remained stable over at least nine months under ambient conditions.

was applied during the fitting for PL, while a linear background correction was used for the E_{22} absorption.

Resonant Raman Scattering and X-ray Photoelectron Spectroscopy. The SWCNTs were precipitated out from solutions and deposited on glass slides for Raman scattering or on gold-coated silicon substrates for XPS measurements. XPS was performed on a Kratos Axis 165 spectrometer at 25 and 175 °C under ultrahigh vacuum (<1 × 10^{-8} Torr). Raman spectra were measured on a LabRAM ARAMIS Raman microscope (Horiba Scientific). The samples were excited with a He−Ne laser (632.8 nm) or a 532 nm laser at a power density of 0.014−0.14 mW μm^{-2}. Each spectrum was obtained by averaging the data collected from three different spots.

Calculation of Inductive Constants. The structure of alkyl-functionalized (6,5)-SWCNTs was constructed using Nanotube Modeler (JCrystalSoft) and HyperChem 8.0 (Hypercube, Inc.). The distance between two atoms and the covalent radius (half of the bond length) were obtained from molecular structures optimized by molecular mechanics.

Density Functional Theory Calculations. The geometries of an 8 nm (2 unit cell) long (6,5)-SWCNT with various quantum defects were optimized using the B3LYP functional in Q-Chem 4. The nanotube ends were terminated with hydrogen atoms to minimize end effects and to avoid the introduction of edge states into the band gap of the nanotube. Most of the calculations considered two alkyl groups (to avoid radical character) covalently attached near the center of the 8 nm nanotube, although single, triple, and higher functionalizations were also considered. DFT with the 6-31G* basis set was used for minimization. Mulliken analysis was performed to reveal the charge distribution around the created defects.

RESULTS AND DISCUSSION

Our starting material is (6,5)-SWCNTs that are 0.75 nm in diameter and typically less than 500 nm (or 125 unit cells) in length. The nanotubes are sorted using gel chromatography[23] to a high level of optical purity and stabilized as individual particles in water or D_2O by 1 wt % SDS. The starting (6,5)-SWCNTs have intrinsic absorption and PL peaks at 979 nm (E_{11}) and 568 nm (E_{22}), which arise from their excitonic transitions.[12,13] Figure 2 shows that covalent attachment of perfluorinated hexyl groups to the nanotubes produces a bright defect PL peak (E_{11}^-) at 1155 nm. The observed peak is red-shifted from the parent nanotube PL (E_{11}) by 177 nm (ΔE = 190 meV), and the full width at half-maximum (fwhm) of the peak increases from 37 to 69 meV. This new feature arises within minutes of the start of the reaction, and the PL intensity plateaus in 25 min (Figure 2c). The bright PL feature remains stable for several months at room temperature. The PL of the alkylated carbon nanotubes shows a strong dependence on the nanotube diameter, d, given by $\Delta E = A/d^2$, where A = 18.7 meV nm^2, suggesting that the new emission peak arises from brightening of dark excitons (Figures S1 and S2).[15] Notably, (6,5)-SWCNT−$(CF_2)_5CF_3$ exhibits PL that is brighter than that of the parent nanotube by more than an order of magnitude (Figure S3).

Correlated measurement of PL, Raman scattering, and X-ray photoelectron spectroscopy (XPS) unambiguously confirmed that the new PL originates from sp^3 quantum defects due to the covalent attachment of a small number of alkyl groups to the sp^2 carbon lattice. The formation of a covalent C−C bond between the alkyl group and the carbon nanotube is evidenced by the rise of the symmetry-breaking, defect-induced Raman scattering of the D phonon (~1300 cm^{-1}).[24] The intensity of this Raman band with respect to the in-plane stretching mode

DOI: 10.1021/jacs.6b03618
J. Am. Chem. Soc. 2016, 138, 6878−6885

(E_{2g}) of the sp^2 bonded carbon lattice (G band, ~1590 cm^{-1}) increases from 0.10 to 0.98 in highly functionalized nanotubes (Figure S4). Both the Raman D/G ratio and the XPS intensity of the perfluoroalkyl group increase in proportion to the relative concentration of alkyl halide. High-resolution XPS of (6,5)-SWCNT−$(CF_2)_5CF_3$ shows the growth of an sp^3 C 1s peak at 285 eV as a shoulder to the sp^2 C 1s peak (284.7 eV), resulting in substantial peak broadening of the C 1s peak (fwhm of 1.46 eV vs 0.83 eV for the starting nanotubes) (Figure S5). The fluorine (F 1s) signal of the functional group remains constant at high temperature (175 °C) under ultrahigh vacuum (<1 × 10^{-8} Torr), in which there are no physisorbed molecules (Figure S6).

By changing the concentrations of the reagents, we were able to control the intensity of the defect PL. The E_{11}^- intensity of (6,5)-SWCNT−$(CF_2)_5CF_3$ peaks at a carbon-to-alkyl halide reactant molar ratio of 1 to 0.4 (Figure 2). Correspondingly, the Raman D/G ratio increases from 0.10 to 0.18, indicating that a small amount of alkyl groups are covalently attached to the nanotubes. Consistent with Raman scattering, the vis−NIR absorption barely decreased. On the basis of XPS (Figure S4), we estimate that the attached −$(CF_2)_5CF_3$ groups are at a density of one group per 166 carbons or 1.8 nm of nanotube length on average. This density is much higher than that produced by diazonium salts[15] and may suggest distinct reaction propagation.[22]

This synthetic quantum system provides exceptional chemical tunability of the near-infrared PL energy. We can continuously red-shift the E_{11}^- emission simply by increasing the number of fluorine atoms along a six-carbon alkyl backbone (Figure 3b and Table 1). The energy shift goes from 133 meV for −$(CH_2)_5CH_3$ to 190 meV for −$(CF_2)_5CF_3$. A consistent trend is observed in a series of partially fluorinated groups in which the distance between the electron-withdrawing moiety ($-CF_3$) and the defect site is varied by changing the chain length, −$(CH_2)_nCF_3$ (n = 0, 1, 2, 3, 4, 5) (Table 1). Larger optical tunability can be achieved by applying diiodo-containing precursors to produce cycloaddition adducts. The "divalent" quantum defects fluoresce even further into the infrared than do the "monovalent" defects (Figure 3c; also see Figure S7). For instance, the PL of (6,5)-SWCNT>CH_2 occurs at 1125 nm, which is red-shifted by 31 meV more than its monovalent counterpart, (6,5)-SWCNT−CH_3. In (6,5)-SWCNT>CF_2, the defect PL is further shifted to 1164 nm, 200 meV to the red of the parent nanotube PL. Divalent aryl defects created by reaction with, for instance, *o*-diiodoaniline and *o*-diiodobenzene also produce new PL peaks that are further red-shifted from the parent nanotube PL by 171 and 190 meV, respectively, in comparison with their monovalent counterparts (Figure 3c and Table 2). These observations demonstrate that the quantum defects can be chemically tailored over a wide range by engineering the functional group that induces the defect state. In Figure 4 we show nine fluorescent quantum defect systems with continuously tunable near-infrared PL and surface functionalities. Additional structures synthesized through these studies are listed in Table S1 in the Supporting Information, demonstrating the excellent chemical and optical tunability of this synthetic quantum system. We note that although the covalent bonding nature of these molecularly tunable fluorescent quantum defects is unambiguous, it remains experimentally challenging to directly determine their detailed atomic configurations on the sp^2 carbon lattice.

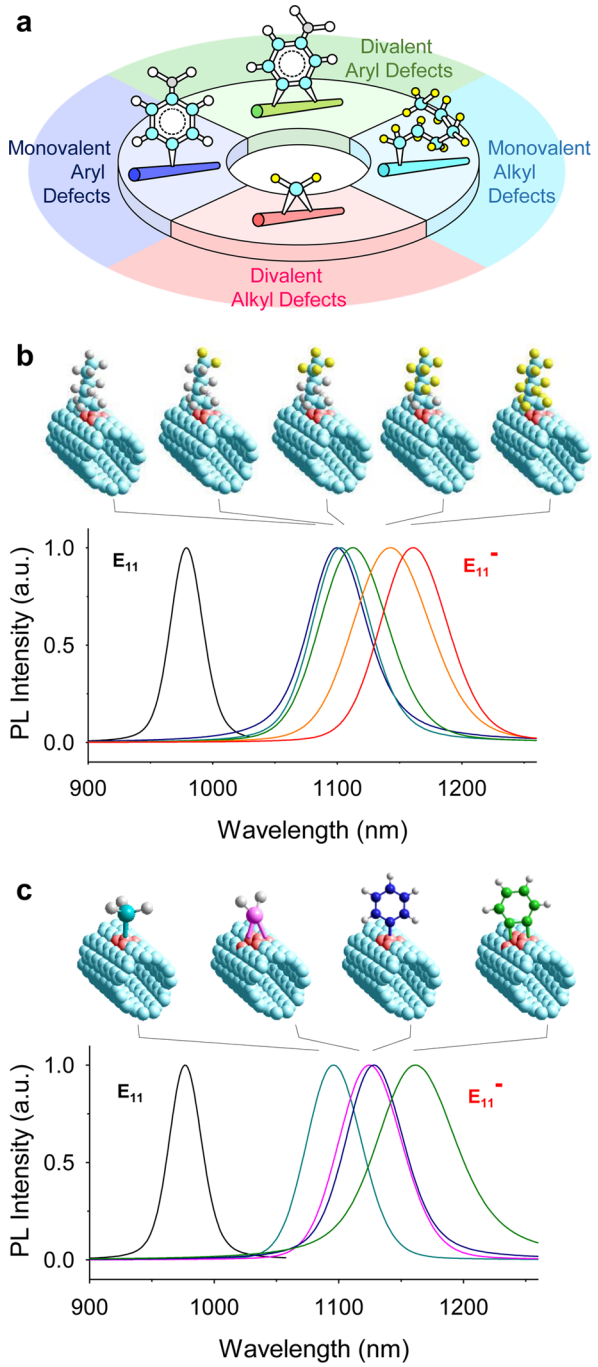

Figure 3. Tunable near-infrared PL from quantum-defect-tailored (6,5)-SWCNTs. (a) Schematic illustration of the four classes of molecularly specific quantum defects that are introduced on a SWCNT by reaction with functional-group-containing halides. (b) PL spectra of (6,5)-SWCNTs functionalized with six-carbon alkyl chains with increasing numbers of fluorine substituents. (c) Comparison of monovalent and divalent fluorescent quantum defects. The nanotubes were excited at 565 nm. The parent exciton PL occurs at 979 nm, while the emission from the quantum defect is systematically tunable by changing the functional group. The spectra were fitted with Voigt functions.

Our experimental results and quantum-chemical theory consistently suggest that this tunability originates from inductive electronic effects associated with the covalently attached functional group. These inductive electronic effects

DOI: 10.1021/jacs.6b03618
J. Am. Chem. Soc. 2016, 138, 6878−6885

Table 1. Spectral Characteristics of Alkyl Fluorescent Quantum Defects in (6,5)-SWCNTs and Calculated Inductive Constants of the Covalently Bonded Alkyl Groups

(6,5)-SWCNT-**R**	E_{11} (nm)	E_{11} fwhm (meV)	E_{11}^- (nm)	E_{11}^- fwhm (meV)	Δ E (meV)	σ* (calc)
Non-functionalized	979	37	-	-	0	-
$-CH_2CH_2CH_2CH_2CH_2CH_3$	981	45	1096	56	133	-0.774
$-CH_2CH_2CH_2CH_2CH_2CF_3$	980	45	1099	56	137	-0.462
$-CH_2CH_2CH_2CH_2CF_2CF_3$	980	38	1107	59	146	-0.127
$-CH_2CH_2CF_2CF_2CF_2CF_3$	983	40	1137	76	170	1.086
$-CF_2CF_2CF_2CF_2CF_2CF_3$	981	42	1155	69	190	4.867
$-CH_2CH_2CH_2CH_2CH_2CF_3$	980	45	1099	56	137	-0.462
$-CH_2CH_2CH_2CH_2CF_3$	979	40	1104	59	143	-0.287
$-CH_2CH_2CH_2CF_3$	980	42	1101	55	140	-0.034
$-CH_2CH_2CF_3$	980	42	1110	59	147	0.310
$-CH_2CF_3$	982	42	1114	67	150	1.244
$-CF_3$	980	45	1158	63	194	3.961

Table 2. PL Spectral Characteristics of (6,5)-SWCNTs Covalently Functionalized with Different Monovalent and Divalent Groups

	monovalent				divalent			
(6,5)-SWCNT-**R**	E_{11} (nm)	E_{11}^- (nm)	Δ E (meV)	(6,5)-SWCNT-**R**	E_{11} (nm)	E_{11}^- (nm)	Δ E (meV)
$-CH_3$ 	980	1094	132	$>CH_2$ 	980	1125	163
$-CF_3$ 	980	1158	194	$>CF_2$ 	980	1164	200
$-C_6H_5$ 	979	1129	168	$>C_6H_4$ 	986	1162	190
$-C_6H_4NH_2$ 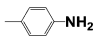	980	1121	159	$>C_6H_3NH_2$ 	980	1133	171

can be described by the empirical Taft constant or inductive constant (σ^*), which quantifies the electronic influence of a substituent along the alkyl chain, excluding resonance effects that also occur in conjugated moieties.[25,26] Consistent with this inductive picture, all of the perfluorinated alkyl defects in (6,5)-SWCNTs, including $-CF_3$, $-(CF_2)_3CF_3$, $-(CF_2)_5CF_3$, and $-(CF_2)_7CF_3$, produce similarly red-shifted E_{11}^- peaks (by 190−194 meV), indicating comparable inductive constants regardless of the carbon chain length (Table S1). For CF_3-terminated alkyl defects, the defect PL energy decreases exponentially with chain length (or approximately the distance from the defect site) (Table 1). Quantitatively, the inductive constants can be calculated using the equation proposed by Cherkasov et al.:[26]

$$\sigma^* = 7.840 \sum_i \Delta\chi_i R_i^2 / r_i^2$$

where $\Delta\chi_i$ is the difference between the electronegativities of ith atom in the substituent and the reaction center, R_i is the covalent radius of the ith atom, and r_i is the distance from this atom to the defect site on a SWCNT. We find that the PL energy shifts are linearly correlated with the calculated inductive constants (σ^*_{calc}) (Figure S8). This linear correlation confirms that the inductive effects associated with the alkyl groups on the fluorescent quantum defects are responsible for the observed energy shifts.

This trend is corroborated by theoretical calculations based on density functional theory (DFT), which consistently predict a larger energy shift for fluorinated alkyl quantum defects than for non-fluorinated ones. DFT calculations were performed on an 8 nm (2 unit cell) long (6,5)-SWCNT using the B3LYP functional with the 6-31G* basis set. For (6,5)-SWCNT−CH_3, the most stable conformation features two methyl groups (avoiding the radical character of a single methyl group) occupying the para positions (Figure S9). We find that the para positions are also energetically favored reaction sites for further methylation. This functionalization pattern follows the distribution of charges around the functional groups (as previously considered[22]). The HOMO−LUMO gap due to the $-CF_3$ defect is 43 meV smaller than that due to $-CH_3$, which is in good agreement with the observed red shift of 62 meV in the defect PL (Table S2). This fluorine substitution effect is not limited to the most thermodynamically stable conformation but is also observed in all of the other possible conformations (Table S2). The calculations also suggest that (6,5)-SWCNT$>CH_2$ and (6,5)-SWCNT$>CF_2$ feature a ring-

DOI: 10.1021/jacs.6b03618
J. Am. Chem. Soc. 2016, 138, 6878−6885

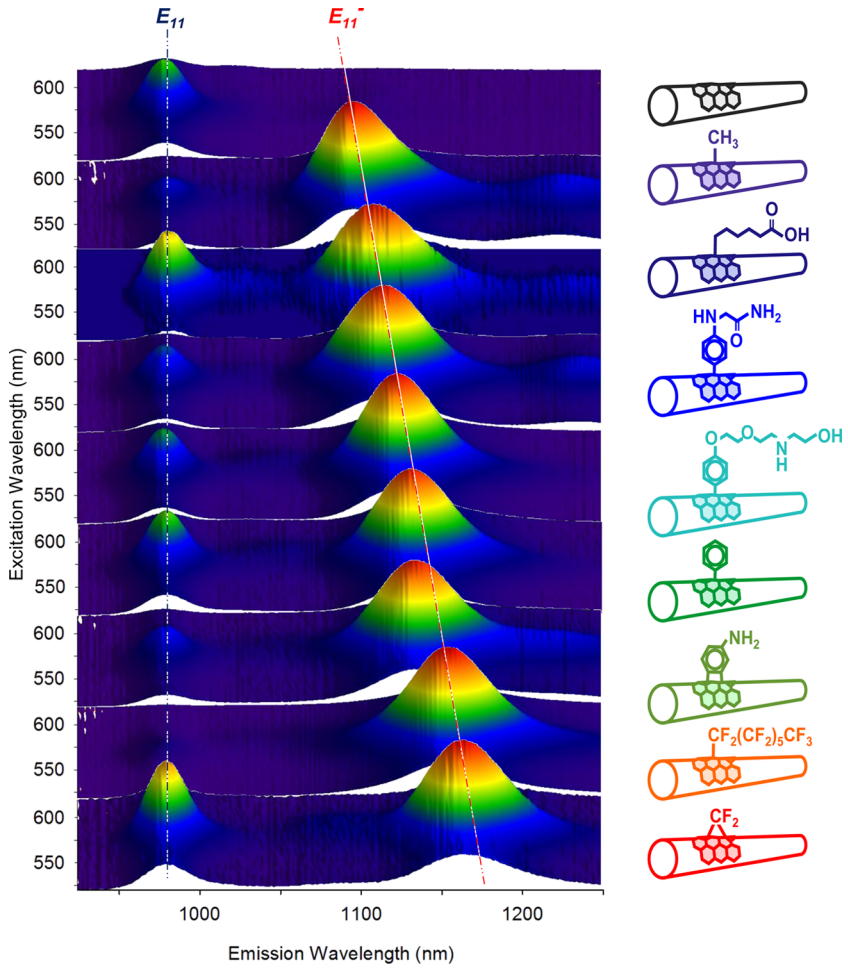

Figure 4. Excitation−emission maps of (6,5)-SWCNTs with chemically tailored fluorescent quantum defects.

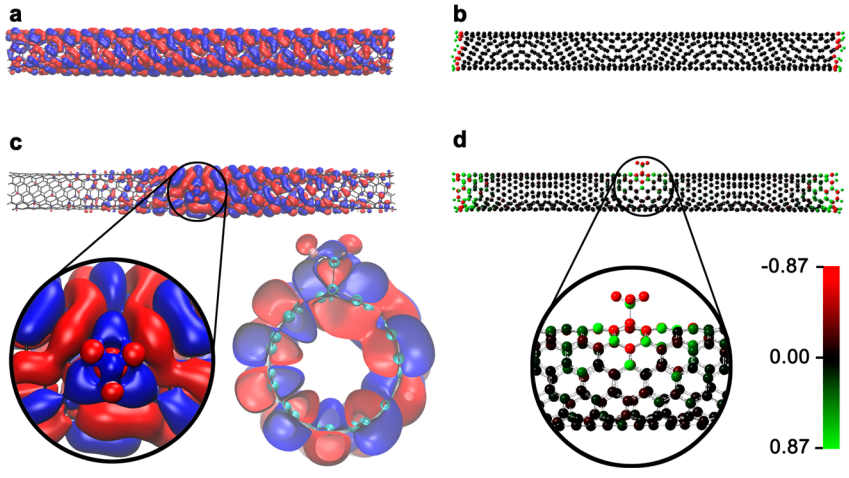

Figure 5. Localization of charges and frontier orbital wave function around a fluorescent quantum defect. (a) HOMO and (b) charge distribution in a pristine (6,5)-SWCNT. The nanotube is free of defects other than its ends, which are terminated with hydrogen atoms to preserve the sp^2 hybridization. (c) HOMO of a (6,5)-SWCNT−CF_3. The inset shows the HOMO for −CF_3 functionalization on a cut perpendicular to the tube. The orbital is plotted at its isosurface equal to 0.003. (d) Positive (green) and negative (red) charges are localized around the covalently attached −CF_3 group. Minor positive and negative charges near zero value are colored in dark.

opened structure that preserves the π conjugation of the nanotube (Figure S10). The breaking of one circumferential C−C bond in the nanotube is ∼1.3 eV more thermodynamically stable than the formation of three-membered-ring-like (cyclopropenyl) adducts along the chiral directions. Mulliken analysis again shows that the charges accumulate preferentially around the defect, driving the subsequent additions of >CH_2 or >CF_2 groups along the longitudinal direction (Figure S11). Consistently, in the presence of a quantum defect, the frontier orbital wave functions of the nanotube become localized to a 2

DOI: 10.1021/jacs.6b03618
J. Am. Chem. Soc. 2016, 138, 6878−6885

nm region around the defect site (Figure 5). This localization effect is less pronounced for divalent defects, suggesting some degrees of tunability by controlling the bonding structure (Figure S12). We note that frontier orbital wave functions are not generally used to describe the excited states of the nanotube. However, our time-dependent DFT calculations suggest that the lowest-energy electronic transition in sp^3 defect-tailored SWCNTs occurs between the HOMO and LUMO (Table S3 and Figures S13 and S14), and hence, the frontier orbitals provide an informative description of the trapped excitons. In all of these systems, this localization effect is distinctly different from defect-free carbon nanotubes, in which the wave function is delocalized and excitons are highly mobile.

We hypothesize that as a result of trapping of excitons at a localized potential well due to a quantum defect, the excitons will respond sensitively to chemical events occurring at the defect site because of the amplification effects of the nanotube, which acts as an antenna.[27] The nanotube antenna harvests light efficiently and channels the generated excitons to the defect site, where the excitons recombine to produce near-infrared PL encoding the chemical information at the functional groups. This picture is supported by titration experiments in which we detected H^+ with both monovalent defects ((6,5)-SWCNT$-C_6H_4NH_2$) and divalent defects ((6,5)-SWCNT$>C_6H_3NH_2$). We find that as the amine moiety switches between the protonated and deprotonated states, the defect PL is shifted by ∼13 meV (Figure S15). This pH switching is not observed in defects that do not contain amines, including $-C_6H_5$ and $>C_6H_4$, confirming the localized nature and the high chemical selectivity of the fluorescent quantum defects.

CONCLUSIONS

We have shown that it is possible to create a new series of quantum systems chemically from semiconducting SWCNTs of the same chirality through molecular engineering of covalently attached functional groups. This new class of synthetic systems is extremely versatile, affording a series of more than 30 chemically well-defined monovalent and divalent quantum defects that show molecule-specific optical and electronic properties distinctly different from those of existing nanostructures. Molecularly tunable fluorescent quantum defects thus add an entirely new dimension to the development of carbon nanomaterials with specific optical and chemical properties. Given the rich molecular moieties and nanotube chirality,[28] one may anticipate that a large variety of near-infrared quantum emitters can now be rationally designed and chemically created for applications ranging from in vivo bioimaging[2] and sensing[4] to room-temperature single-photon sources.[29]

ASSOCIATED CONTENT

Supporting Information

The Supporting Information is available free of charge on the ACS Publications website at DOI: 10.1021/jacs.6b03618.

Raman scattering, XPS, and PL spectra, Mulliken charge distributions, computed orbital energies and bond lengths, frontier orbitals, and time-dependent DFT calculation results (Figures S1−S15 and Tables S1−S3) (PDF)

AUTHOR INFORMATION

Corresponding Authors

*yhw@umd.edu

*schatz@chem.northwestern.edu

Notes

The authors declare no competing financial interest.

ACKNOWLEDGMENTS

This work was supported in part by NSF (CHE-1507974, CAREER CHE-1055514), NIH/NIGMS (1R01GM114167), and AFOSR (MURI FA9550-16-1-0150). A.F. and G.C.S. were supported by NSF (CHE-1465045) and AFOSR (FA9550-14-1-0053). Y.G. was supported by NNSFC (21421002, 21172241) and NBRPC (2012CB821600). We thank K. Gaskell and D. Ramsdell for assistance with XPS experiments, Y. Piao for help with initial spectroscopy experiments, and J. T. Fourkas and M. Ouyang for useful discussions.

REFERENCES

(1) Scholes, G. D.; Rumbles, G. *Nat. Mater.* **2006**, *5*, 683.
(2) Hong, G.; Lee, J. C.; Robinson, J. T.; Raaz, U.; Xie, L.; Huang, N. F.; Cooke, J. P.; Dai, H. *Nat. Med.* **2012**, *18*, 1841.
(3) Chan, W. C. W.; Nie, S. *Science* **1998**, *281*, 2016.
(4) Heller, D. A.; Jeng, E. S.; Yeung, T.-K.; Martinez, B. M.; Moll, A. E.; Gastala, J. B.; Strano, M. S. *Science* **2006**, *311*, 508.
(5) Kamat, P. V. *J. Phys. Chem. C* **2008**, *112*, 18737.
(6) Shirasaki, Y.; Supran, G. J.; Bawendi, M. G.; Bulović, V. *Nat. Photonics* **2013**, *7*, 13.
(7) Rossetti, R.; Nakahara, S.; Brus, L. E. *J. Chem. Phys.* **1983**, *79*, 1086.
(8) Alivisatos, A. P. *Science* **1996**, *271*, 933.
(9) Yin, Y.; Alivisatos, A. P. *Nature* **2005**, *437*, 664.
(10) Gruber, A.; Dräbenstedt, A.; Tietz, C.; Fleury, L.; Wrachtrup, J.; von Borczyskowski, C. *Science* **1997**, *276*, 2012.
(11) Erwin, S. C.; Zu, L.; Haftel, M. I.; Efros, A. L.; Kennedy, T. A.; Norris, D. J. *Nature* **2005**, *436*, 91.
(12) O'Connell, M. J.; Bachilo, S. M.; Huffman, C. B.; Moore, V. C.; Strano, M. S.; Haroz, E. H.; Rialon, K. L.; Boul, P. J.; Noon, W. H.; Kittrell, C.; Ma, J.; Hauge, R. H.; Weisman, R. B.; Smalley, R. E. *Science* **2002**, *297*, 593.
(13) Wang, F.; Dukovic, G.; Brus, L. E.; Heinz, T. F. *Science* **2005**, *308*, 838.
(14) Ghosh, S.; Bachilo, S. M.; Simonette, R. A.; Beckingham, K. M.; Weisman, R. B. *Science* **2010**, *330*, 1656.
(15) Piao, Y. M.; Meany, B.; Powell, L. R.; Valley, N.; Kwon, H.; Schatz, G. C.; Wang, Y. *Nat. Chem.* **2013**, *5*, 840.
(16) Wang, Q. H.; Strano, M. S. *Nat. Chem.* **2013**, *5*, 812.
(17) Akizuki, N.; Aota, S.; Mouri, S.; Matsuda, K.; Miyauchi, Y. *Nat. Commun.* **2015**, *6*, 8920.
(18) Brozena, A. H.; Leeds, J. D.; Zhang, Y.; Fourkas, J. T.; Wang, Y. *ACS Nano* **2014**, *8*, 4239.
(19) Ma, X.; Adamska, L.; Yamaguchi, H.; Yalcin, S. E.; Tretiak, S.; Doorn, S. K.; Htoon, H. *ACS Nano* **2014**, *8*, 10782.
(20) Zhang, C.-P.; Chen, Q.-Y.; Guo, Y.; Xiao, J.-C.; Gu, Y.-C. *Chem. Soc. Rev.* **2012**, *41*, 4536.
(21) Zhang, Y.; Valley, N.; Brozena, A. H.; Piao, Y.; Song, X.; Schatz, G. C.; Wang, Y. *J. Phys. Chem. Lett.* **2013**, *4*, 826.
(22) Deng, S.; Zhang, Y.; Brozena, A. H.; Mayes, M. L.; Banerjee, P.; Chiou, W. A.; Rubloff, G. W.; Schatz, G. C.; Wang, Y. *Nat. Commun.* **2011**, *2*, 382.
(23) Liu, H.; Nishide, D.; Tanaka, T.; Kataura, H. *Nat. Commun.* **2011**, *2*, 309.
(24) Dresselhaus, M. S.; Dresselhaus, G.; Jorio, A. *J. Phys. Chem. C* **2007**, *111*, 17887.
(25) Hansch, C.; Leo, A.; Taft, R. W. *Chem. Rev.* **1991**, *91*, 165.

DOI: 10.1021/jacs.6b03618
J. Am. Chem. Soc. 2016, 138, 6878−6885

(26) Cherkasov, A. R.; Galkin, V. I.; Cherkasov, R. A. *Russ. Chem. Rev.* **1996**, *65*, 641.
(27) Kwon, H.; Kim, M.; Meany, B.; Piao, Y.; Powell, L. R.; Wang, Y. *J. Phys. Chem. C* **2015**, *119*, 3733.
(28) Tu, X.; Manohar, S.; Jagota, A.; Zheng, M. *Nature* **2009**, *460*, 250.
(29) Ma, X.; Hartmann, N. F.; Baldwin, J. K. S.; Doorn, S. K.; Htoon, H. *Nat. Nanotechnol.* **2015**, *10*, 671.
(30) Zheng, M.; Diner, B. A. *J. Am. Chem. Soc.* **2004**, *126*, 15490.

■ NOTE ADDED AFTER ASAP PUBLICATION

Due to a production error, this paper was published on the Web on May 17, 2016, with minor errors in the caption for Figure 2 and ref 21. The corrected version was reposted on May 19, 2016.

DOI: 10.1021/jacs.6b03618
J. Am. Chem. Soc. 2016, 138, 6878−6885